A biomechanical model of swallowing for understanding the influence of saliva and food bolus viscosity on flavour release

Clément de Loubens, Albert Magnin, Marion Doyennette, Ioan Cristian Tréléa, Isabelle Souchon

www.elsevier.com/locate/yjtbi

A biomechanical model of swallowing for understanding the influence of saliva and food bolus viscosity on flavour release

Clément de Loubens, Albert Magnin, Marion Doyennette, Ioan Cristian Tréléa, Isabelle Souchon

PII: S0022-5193(11)00216-5
DOI: doi:10.1016/j.jtbi.2011.04.016
Reference: YJTBI6447

To appear in: *Journal of Theoretical Biology*

Received date: 28 January 2011
Revised date: 10 April 2011
Accepted date: 15 April 2011

Cite this article as: Clément de Loubens, Albert Magnin, Marion Doyennette, Ioan Cristian Tréléa and Isabelle Souchon, A biomechanical model of swallowing for understanding the influence of saliva and food bolus viscosity on flavour release, *Journal of Theoretical Biology*, doi:10.1016/j.jtbi.2011.04.016

A biomechanical model of swallowing for understanding the influence of saliva and food bolus viscosity on flavour release

Clément de Loubens[a,b,*], Albert Magnin[c], Marion Doyennette[a,b], Ioan Cristian Tréléa[b,a], Isabelle Souchon[a,b]

Journal of Theoretical Biology

[a] INRA, UMR 782 Génie et Microbiologie des Procédés Alimentaires, CBAI 78850 Thiverval Grignon, France

[b] AgroParisTech, UMR 782 Génie et Microbiologie des Procédés Alimentaires, CBAI 78850 Thiverval Grignon, France

[c] Laboratoire de Rhéologie, Université Joseph Fourier-Grenoble I, Grenoble INP, CNRS (UMR 5520), BP 53, Domaine Universitaire, 38041 GRENOBLE cedex 9, France

∗Corresponding author

Email addresses: cdeloubens@grignon.inra.fr (Clément de Loubens), magnin@ujf-grenoble.fr (Albert Magnin), souchon@grignon.inra.fr (Isabelle Souchon)

Abstract

After swallowing a liquid or a semi-liquid food product, a thin film responsible for the dynamic profile of aroma release coats the pharyngeal mucosa. The objective of the present article was to understand and quantify physical mechanisms explaining pharyngeal mucosa coating. An elastohydrodynamic model of swallowing was developed for Newtonian liquids that focused on the most occluded region of the pharyngeal peristaltic wave. The model took lubrication by a saliva film and mucosa deformability into account. Food bolus flow rate and generated load were predicted as functions of three dimensionless variables: the dimensionless saliva flow rate, the viscosity ratio

between saliva and the food bolus, and the elasticity number. Considering physiological conditions, the results were applied to predict aroma release kinetics.

Two sets of conditions were distinguished. The first one was obtained when the saliva film is thin, in which case food bolus viscosity has a strong impact on mucosa coating and on flavour release. More importantly, we demonstrated the existence of a second set of conditions. It was obtained when the saliva film is thick and the food bolus coating the mucosa is very diluted by saliva during the swallowing process and the impact of its viscosity on flavour release is weak. This last phenomenon explains physically *in vivo* observations for Newtonian food products found in the literature. Moreover, in this case, the predicted thickness of the mix of food bolus with saliva coating the mucosa is approximately of 20 µm; value in agreement with orders of magnitude found in the literature.

Keywords: lubrication, pharynx, elastohydrodynamic, aroma, texture, model

36

37 1. Introduction

38 Food formulation has to take different recommendations to improve nutritional quality of foods (low
39 fat content, less salt and sugar) and to adapt food to specific people (as disphagic patients) without
40 modifying their organoleptic qualities (flavour and texture perception). These organoleptic qualities
41 are closely related to the physiological process of food transformation during chewing and
42 swallowing (Weel et al., 2004; Boland et al., 2006). It is so necessary to study the processes of food
43 bolus formation (Woda et al., 2010 ; Yven et al., 2010) and of swallowing mechanisms in relation with
44 physical properties of food (Taniguchi et al., 2008; Tsukada et al., 2009) to formulate novel food
45 products.

46 Swallowing of a liquid or a semi-liquid food product generates a thin film of product coating the
47 pharyngeal mucosa (Levine, 1989) responsible for the dynamic profile of aroma release (Buettner et
48 al., 2001). The influence of rheology of liquid and semi-liquid food products on aroma release and
49 perception is an unclear and debatable issue in the literature (Hollowood et al., 2002; Cook et al.,
50 2003; Weel et al., 2004; Saint-Eve et al., 2006). We can assume that the conclusions did not match
51 because the experimental investigations covered very different rheological properties (from yield
52 stress fluids as yoghurt to shear-thinning fluids as hydrocolloids). Moreover, these analyses may have
53 been biased by the fact that rheological properties and physico-chemical properties governing aroma
54 relase (such as mass transfer coefficient, Tréléa et al., 2008) are often coupled properties of the
55 product. To explain the role of product rheology on aroma release, we need to study the physical
56 phenomena governing pharyngeal mucosa coating.

57 To understand these phenomena, de Loubens et al. (2010) analysed the physiology and
58 biomechanics of swallowing. They showed that the thin film of product coating the mucosa is due to
59 a weak reflux during the pharyngeal peristalsis between the root of the tongue and the posterior

pharyngeal wall (Figure 1a). To physically represent this phenomenon and simplify the problem, they focused their attention on the most occluded region of the peristaltic wave. In this region, the pharyngeal peristalsis wave is equivalent to a forward roll coating process. Based on this physiological analysis, a fluid-mechanical model that considers lubrication by a saliva film was developed. However, mucosa deformability was not considered in their first model, whereas it is an important phenomena that may quantitatively improve the model predictions. In the present study, we consider that the pharyngeal peristalsis is equivalent to a forward roll coating process with deformable and lubricated surfaces (Figure 1b). In this process, the mucosa deform under the load L' applied by the pharyngeal constrictors muscles (Figure 1b). The purpose of this study was to develop an elastohydrodynamic model of the pharyngeal peristalsis in order to understand and quantify the role of saliva and the food bolus on the pharyngeal mucosa coating. The equation system was scaled by the elastic effects and solved numerically. A parametric study showed the influence of the different model parameters on food bolus flow rates and generated forces. The model was applied to flavour release and the predictions were compared with *in vivo* observations obtained for Newtonian liquid foods from the literature. Finally, main model assumptions were discussed.

2. Elastohydrodynamic model of the pharyngeal peristalsis

2.1. Model hypothesis

As de Loubens et al. (2010), we considered that the swallowing process is equivalent to a forward roll coating process (Figure 1). Moreover, we took the deformability of the mucosa into account. The general features of the forward roll coating process with deformable rolls for Newtonian fluids have been described by Coyle (1988). This author analysed the flow by means of two dimensionless numbers: the elasticity parameter E_s is the ratio of viscous to elastic forces:

$$E_s = \frac{\mu_0 ' U '}{(2R')^2 E_e '} \quad (1)$$

and the load parameter F is the ratio of the external load to the elastic forces:

$$F = \frac{L'}{(2R')^2 E_e'} \quad (2)$$

where E_e' is the effective elastic modulus of the substrate that covers the deformable rolls (Pa/m), μ' the viscosity of the fluid (Pa.s), R' the rolls radius (m), U' the velocity (m/s) and L' the applied load per unit of width (N/m).

Two limiting cases can be distinguished (Johnson, 1970). When F is low and E_s is high, the viscous forces predominate. This case tends to the rigid roll limit that was the case developed for pharyngeal peristalsis by de Loubens et al. (2010). When F is high and E_s is low, the elastic forces dominate and the pressure profile is similar to that of a dry contact. This case is the large deflection limit. The cylinders surfaces would intersect if there were no deformation. Coyle (1988) defined the effective elastic modulus by $E_e' = E'/e_m'$, where E' is the Young modulus of the substrate (Pa) and e_m' its thickness (m). Useful physiological data on the pharyngeal peristalsis are given in Table 1. From these data and the results obtained by Coyle (1988), we can estimate that the pharyngeal peristalsis occurs on the large deflection limit ($F \approx 3.10^{-5}$ and $E_s \approx 8.10^{-9}$), although the parameters have a wide range of variation.

The present physical situation is therefore modeled with the lubrication approximation: the inertial terms are neglected compared to the viscous terms in the Navier-Stokes equations. The use of the lubrication approximation for the most occluded region of the pharyngeal peristalsis wave and the fact that the flow can be considered as stationary was already justified by de Loubens et al. (2010). In addition, we take the presence of a lubricating saliva film and mucosa deformability into consideration.

Since the confusion concerning the role of food rheology on flavour release, we restrict our analysis to homogeneous Newtonian food bolus. Moreover, in the paragraph concerning the model

applications (4.2), model predictions were compared with *in vivo* data obtained with Newtonian glucose solutions. As demonstrated by de Loubens et al. (2010), the main role of saliva during swallowing is to obstruct the contact. To represent this phenomenon, saliva is considered as being a Newtonian fluid too.

The geometry is symmetric along the x-axis (Figure 2). Relative quantities associated with saliva and the food bolus are referred to as 1 and 2, respectively. Between the two fluids, we ignored diffusion and surface tension effects. The dimensional values are identified by the symbol '. The flow rate of saliva q_1' (m^3/s) is assumed to be known and the flow rate of the food bolus q_2' is calculated. μ_i' (Pa.s) refers to the viscosities, e_m' the thickness (m) of the deformable layer of mucosa, H'(x) the half gap between the two cylinders (m), H_0' the "negative-gap width" (m), $h_2'(x)$ the location of the interface between the food bolus and saliva (m), U' the cylinder velocity (m/s), L' the load per unit of width (N/m), and R' the radius (m).

2.2. Elastic model of the mucosa

Near the contact point, the undeformed roll surface profiles are locally approximated by parabolas:

$$H'(x') = -H_0 + \frac{x'^2}{2R'} + \Delta H'(x') \quad (3)$$

where ΔH'(x') is the cylinder surface deflection and must be expressed in terms of model for the elastic deformation of the rolls. The deformation of the layer can be considered with different models. Skotheim and Mahadevan (2005) have carried out a detailed study of fluid-immersed compressible, incompressible and poro-elastic soft interfaces. The one-dimensional Constrained Column Model (CCM) is the most tractable and the least intensive at the computational level. It assumes that the local pressure p' is directly proportional to the local deflection ΔH':

$$\Delta H'(x') = \frac{p'(x')}{E_e} \quad (4)$$

For large deflections and incompressible compliant layers such as mucosa, Carvalho and Scriven (1995) and Gostling et al. (2003) have proposed:

$$E_e' = \frac{4E'}{e_m'} \quad (5)$$

They found good agreement between this model and most of the sophisticated models in terms of the flow rates and the generated forces. These two last assumptions were retained to model the surface deflection (Eq. 4 and 5).

2.3. Dimensionless variables

For high load, viscous forces are small compared to elastic forces, so the pressure should be scaled with the latter. Choosing H'_0 as the length scale is the most convenient choice because it allows the model to be written in two parameters only, namely the viscosity ratio:

$$\alpha = \frac{\mu'_2}{\mu'_1} \quad (6)$$

and the elasticity number:

$$N_e = E_S \left(\frac{2R'}{H'_0} \right)^{5/2} \quad (7)$$

where E_s is defined with the saliva viscosity: $E_S = \frac{\mu'_1 U'}{(2R')^2 E'_e}$.

The limit Ne→+∞ corresponds to the case where the undeformed rolls would touch. The limit Ne→0 corresponds to the dry rolling contact. The dimensionless values defined for imposed velocity and gap are given by:

$$x = \frac{x'}{\sqrt{2R'H'_0}}$$

146 $$z = \frac{z'}{H'_0}$$

147 $$u_i = \frac{u'_i}{U'}$$

148 $$q_i = \frac{q'_i}{U' H'_0}$$

149 $$p_i = \frac{p'_i}{E'_e H'_0}$$

150 $$L = \frac{L'}{E'_e H'_0 \sqrt{2R' H'_0}}$$

151 *2.4. Hydrodynamic model*

152 The cylinder profile is given by:

153 $$H(x) = -1 + x^2 + p(x) \quad (8)$$

154 The momentum conservation equations are solved in the lubrication approximation in their
155 dimensionless form:

156 $$\frac{\partial p}{\partial x} = N_e \frac{\partial^2 u_1}{\partial z^2} \quad (9)$$

157 $$\frac{\partial p}{\partial x} = \alpha . N_e \frac{\partial^2 u_2}{\partial z^2} \quad (10)$$

158 $$\frac{\partial p}{\partial z} = 0 \quad (11)$$

159 Defining η = z/H(x) and β = h_2(x)/H(x), and considering no wall slip, continuity of velocity and shear
160 stress at the interface between the food bolus and the saliva and symmetry, the boundary conditions
161 are:

$$u_1(\eta = 1) = 1 \quad (12)$$

$$u_1(\eta = \beta) = u_2(\eta = \beta) \quad (13)$$

$$\left.\frac{\partial u_1}{\partial \eta}\right|_{\eta=\beta} = \alpha \left.\frac{\partial u_2}{\partial \eta}\right|_{\eta=\beta} \quad (14)$$

$$\left.\frac{\partial u_2}{\partial \eta}\right|_{\eta=0} = 0 \quad (15)$$

After integration of (9) and (10), application of the boundary conditions (12), (13), (14) and (15) and of the mass conservation, the flow rates are given by:

$$q_1 = \frac{H^3(\theta)}{2N_e}\cos^2(\theta)\frac{dp}{d\theta}\left[-\frac{\beta^3}{3} + \beta - \frac{2}{3}\right] + H(\theta)(1-\beta) \quad (16)$$

$$q_2 = \frac{H^3(\theta)}{2N_e}\cos^2(\theta)\frac{dp}{d\theta}\left[\beta^3\left(1 - \frac{2}{3\alpha}\right) - \beta\right] + H(\theta)\beta \quad (17)$$

where θ = arctan(x) .

Upstream, we consider that the contact is fully submerged. Downstream, the film splits. In the large deflection case, Coyle (1988) has demonstrated that this boundary condition has a slight effect on the results, so we consider that:

$$p\left(-\frac{\pi}{2}\right) = p\left(\frac{\pi}{2}\right) = 0 \quad (18)$$

After resolution, we calculate the resulting load:

$$L = \int_{-\frac{\pi}{2}}^{\frac{\pi}{2}} \frac{p(\theta)}{\cos^2(\theta)} d\theta \quad (19)$$

177 *2.5. Resolution method*

178 From (16) and (17), we obtain an algebraic equation:

179 $$\frac{2}{3}H(\theta)\left(1-\frac{1}{\alpha}\right)\beta^4+\left[\left(q_1-H(\theta)\right)\times\left(1-\frac{2}{3\alpha}\right)+\frac{q_2}{3}\right]\beta^3+\left[\frac{H}{3}-q_1-q_2\right]\beta+\frac{2}{3}q_2=0 \quad (20)$$

180 and a differential equation on the pressure:

181 $$\frac{dp}{d\theta}=\frac{3Ne\left(q_1+q_2-H(\theta)\right)}{H(\theta)^3\cos(\theta)^2\left[\beta^3\left(1-\frac{1}{\alpha}\right)-1\right]} \quad (21)$$

182 Where

183 $$H(\theta)=-1+\tan(\theta)^2+p(\theta) \quad (22)$$

184 Equations (20), (21) and (22) were solved using Matlab7 software. Even so, the integration had to be
185 performed backwards in space (from π/2 to -π/2) to obtain numerical stability. q_2 is the unknown
186 variable. For a set of parameters (q_1, α, Ne), we iterated on q_2 until the boundary conditions (18)
187 were verified.

188 **3. Parametric study**

189 *3.1. Mono-layer case*

190 Numerical solutions were validated by comparing the results in the monolayer case with those of
191 Coyle (1988). Figure 3 shows the flow rate q_1 and the load L as a function of the elasticity number N_e.
192 As shown by Coyle (1988), from the results presented Figure 3, the flow rate and load dependence
193 with N_e can be approximated by the relationships:

194 $q_1 \approx 0.5N_e^{0.5}$ when $q_2=0$ (23)

195 $L \approx 1.3+1.7N_e^{0.55}$ when $q_2=0$ (24)

When N_e tends to zero, the flow rate decreases and the load tends to 1.3. This value corresponds to a dry rolling contact and was verified analytically (Coyle, 1988).

3.2. Food bolus flow rates

Figure 4-a shows the influence of Ne and Figure 4-b the influence of the saliva flow rates q_1 at N_e=1 on the food bolus flow rates q_2 for different cases. The food bolus flow rate q_2 decreases when N_e tends to zero corresponding to the dry rolling contact. When there is no saliva at the interface (q_1=0), q_2 dependence with Ne and α can be expressed with a relationship similar to (23):

$$q_2 \approx 0.5(\alpha N_e)^{0.5} \text{ when } q_1 = 0 \quad (25)$$

Increasing the viscosity ratio α increases q_2 whereas saliva lubrication decreases q_2. The influence of the saliva flow rate q_1 decreases when N_e increases. When the relationship:

$$N_e \approx 4q_1^2 \quad (26)$$

is verified, the contact is over-flooded by saliva and q_2 tends to zero.

The viscosity ratio α has a strong influence on the food bolus flow rate q_2 when the saliva flow rate q_1 is low. Its impact drop sharply when q_1 increases.

3.3. Load

Figure 5-a shows the influence of N_e and Figure 5-b the influence of q_1 at Ne=1 on the generated load L for different cases. When the contact is not lubricated by saliva, we obtain a relationship equivalent to (24):

$$L \approx 1.3 + 1.7(\alpha N_e)^{0.55} \text{ when } q_1 = 0 \quad (27)$$

When α increases, L increases. When α is smaller than 1, L decreases with q_1, whereas L increases with q_1 when α is higher than 1. The dependence of L on q_1 is highly reduced when N_e is weak due to the fact that the contribution of hydrodynamic pressure to the load is negligible.

3.4. Pressure and gap profiles

Figure 6 shows pressure (a and b) and gap profiles (c and d) for N_e=1 and N_e=10^{-3} for different cases. The pressure sharply increases as the fluid is dragged into the narrowing channel, after which the channel widens and the pressure drops. When α is higher than 1 the pressure profile developed with α and the saliva flow rate q_1 reduces its development and, inversely, when α is lower than 1. When Ne is weak, the pressure profile is less dependent on α and q_1 as shown in Figure 6-b for Ne = 10^{-3}. It tends to a parabola corresponding to a dry rolling and the surfaces are more and more parallel and closer (Coyle, 1988): the pressure profile is dominated by the elastic deformation of the mucosa.

4. Applications

The aim of this section is to provide quantitative results for typical physiological parameters, to apply these results to *in vivo* aroma release and to compare the predictions with *in vivo* experiments found in the literature.

4.1. Application to swallowing

Coating flows often present instabilities and the film varies in a wavy, sinusoidal-like manner across the substrate. This type of film thickness non-uniformity is usually referred to as ribbing. It is a consequence of an imbalance between surface tension forces and the pressure gradient present within the downstream nip region that generate vortex in the film-split region. In the case of a bi-layer coating, the two fluids are mixed together under the vortex action at the contact output. Chong et al. (2007) observed that ribbing is present over a wide range of operating parameters for negative gaps. We can thus consider that ribbing and vortex occur during swallowing and that the food bolus is therefore mixed with the saliva film. The interesting model outputs in terms of flavour release are

239 the total thickness e' of the mixture of the food bolus with saliva ($e'=e'_1+e'_2$) and the rate of dilution r
240 of the food bolus in saliva defined by:

241 $$r = 100\,\frac{e_2'}{e_1'+e_1'} \quad (28)$$

242 In order to apply the model to pharyngeal peristalsis, the mathematical model was used to calculate
243 the thickness of bolus e'_2 deposited on the pharyngeal mucosa at imposed velocity U' and load L'. A
244 value of L' to be reached was fixed and (20), (21) and (22) were solved as explained in 2.5. We
245 iterated on q'_2 and H'_0 until (18) and (19) were verified. In fact, the action of the pharyngeal
246 constrictors muscles is equivalent to setting a normal force on the rolls, refferd to as load L' (de
247 Loubens et al., 2010).

248 Figure 7 shows the total thickness (in µm) as a function of the rate of dilution (in %) for different
249 parameters representative of different physiological conditions (Table 1).

250 Regardless of the parameters, the values of the elasticity number N_e are lower than the 1 and, as
251 previously explained, the situation is therefore similar to the dry rolling contact. The load is due to
252 the elastic forces and not to the hydrodynamic pressure.

253 When the viscosity ratio α is 1 (cases a1, b1, c1), the deposited thickness is constant regardless of the
254 dilution rate is. When the viscosity ratio increases (comparison between the cases a1 and a10, for
255 example), there are two sets of conditions. The first one is obtained when the food bolus is not very
256 diluted with saliva (r → 0%) and the viscosity ratio has a considerable influence on the total thickness
257 e'. The second one is obtained when the food bolus dilution increases (r → 100%) and the total
258 thickness tends to a constant.

259 In the cases a1, the rate of dilution between the two sets of conditions is about 45%, resulting in an
260 initial saliva thickness e'_1 of approximately 5 µm.

When the dilution ratio is maximal, the saliva entirely obstructs the contact and the bolus cannot coat the mucosa. The limit value of saliva thickness is approximately 10 µm in the case a.

The comparison between cases a and b illustrates the strong role of the peristalsis wave velocity U' When U' is multiplied by 5, the total thickness is multiplied by 2.5. Moreover, the limit rate of dilution r and the limit of saliva thickness between the two sets of conditions previously described increase when the wave velocity increases: in case a they are about 45% and 5 µm and 55% and 15 µm in case b. The saliva thickness value necessary to over-flood the contact increases from about 10 to 25 µm (r = 100%) as well.

The comparison of cases a10 and c10 shows that increasing the Young modulus of the mucosa E' reduces the total thickness. The values of E' reported in Table 1 have one decade of difference. This parameter is difficult to obtain *in vivo* and we have therefore used the Young modulus obtained from human skin *in vivo* (Diridollou et al., 2000) and of human pharyngeal tissue in *post mortem* tension (Kim et al., 1998). The mechanical behavior of the mucosa would require more considerations. In fact, mucosa presents a viscoelastic behavior (Kim et al., 1998) and, as a result, the Young modulus obtained at the time scale of the process should be introduced into the model (Cohu and Magnin, 1997).

4.2. Application to flavour release

Predictions of aroma release kinetics

The results of the pharyngeal mucosa coating model were used in a mechanistic model that predicts aroma release (Doyennette et al., 2011). Figure 8 shows the kinetics of aroma release in the nasal cavity predicted by the mechanistic model for different viscosity ratio α and rates of dilution r calculated with the present model. In this section, we considered that the physico-chemical properties of the food bolus are independent of its viscosity.

Two sets of conditions can be distinguished according to the physiological parameters and the viscosity ratio. When the initial thickness of saliva and the dilution are weak (r→0%, cases 3 and 4), viscosity has a considerable effect on the decreasing part of the aroma release kinetics, whereas when the dilution with saliva is strong (r→100%, cases 1 and 2), viscosity has no effect on aroma release. Figure 7, we show that for typical physiological parameters and a food bolus viscosity of 50 mPa.s, the order of magnitude of the limit value of saliva thickness that distinguishes the two cases is between 5 and 15 µm.

Comparison with in vivo aroma release kinetics

In this section, the model predictions are compared with the results obtained in the literature.

Doyennette et al. (2011) carried out an *in vivo* investigation of the influence of viscosity on aroma release. They used glucose solutions as test fluids that varied widely in viscosity (from 0.7 to 405 mPa.s at 35◦C). They concluded that the solution coating the pharyngeal mucosa was highly diluted with saliva. To show this, they compared the maximal relative concentration of kinetics C_{max} obtained *in vivo* with their model predictions for two different cases.

Figure 9 shows the maximal concentration of kinetics C_{max} obtained *in vivo* and predicted by the model in two different cases as a function of the viscosity of the glucose solution. They observed a maximal difference of 40% *in vivo* on C_{max}, depending on the glucose viscosity of the solution. However, when they simulated aroma release kinetics by considering that the residual thickness of the product was not diluted by saliva (r=0%), they observed differences of 97% between the products whereas, when they considered a rate of dilution r of approximately 85%, their predictions were in agreement with the *in vivo* observations. Thus, it was necessary to suppose that the food bolus was highly diluted by saliva to explain the *in vivo* observations.

The biomechanical model developed in the present study makes it possible to understand the physical origins of these observations: the initial thickness of saliva coating the mucosa is sufficiently

thick to dilute the food bolus coating the mucosa at the level of the most occluded region of the pharyngeal peristaltic wave and to break the viscosity influence on coating and flavour release. Moreover, the thickness of the residual film that coats the mucosa after swallowing was estimated at approximately 15 µm in their study and this value is close to those calculated with the present model (Figure 7).

5. Discussion about non-Newtonian behavior

In despite of different assumptions performed in the model, this last is able to explain the physical origins of *in vivo* observations for Newtonian fluids. The main assumptions concern the physical fluids properties (saliva and food bolus) and especially their rheological behavior that we discuss in this section.

5.1. Rheology of saliva

In the present model of pharyngeal peristalsis, saliva was considered as a Newtonian fluid although it presents complex rheological properties as shear thinning behavior (Stokes et al., 2007), viscoelasticity (Stokes et al., 2007), extensional viscosity (Harward et al., 2010) and normal stress (Stokes et al., 2007). Moreover, the intensity of its properties depends greatly upon the method of stimulation (Stokes et al., 2007).

To discuss about the interest to consider shear thinning behavior in the model, Figure 10 shows the shear rate distribution (calculated by the present model) in the contact between the root of the tongue and the posterior pharyngeal wall for different levels of lubrication by saliva and for mean physiological conditions. When saliva thickness increases, mucosa are more and more close and parallel. At the interface between the food bolus and the saliva, there is a gap of shear stress due to the continuity of shear stress and the difference of viscosity between the two fluids. For the different cases, shear rates vary between 1 and 10^4 s^{-1}, approximately. Stokes et al. (2007) shows that the shear viscosity of saliva vary at maximum between 20 and 1 mPa.s for shear rates comprise between

2 and 5.10^3 s^{-1}. These variations are relatively important; knowing that, the thickness of product varies with the square of the viscosity in the monolayer case. At the light of the present results, the shear thinning behavior of saliva should change quantitatively the model predictions.

Saliva has a highly elastic nature (Stokes et al., 2007) that has to be compared to the time scale of the coating process during swallowing. This time scale is given by the ratio l'/U', where l' is the length of the contact (≈10 mm, Figure 10), is about 20 ms. For saliva, Stokes et al. (2007) reported that the relaxation times of saliva are from 30 ms to 1 s. Being superior to the time scale of the pharyngeal mucosa coating process, viscoelasticity can have an influence on the coating phenomena.

Saliva presents also an extensional viscosity μ_E' (Harward et al., 2010). According to the results of Harward et al. (2010), the extensional viscosity depends on the strain rate and can reach 120 times the shear viscosity. In the momentum conservation equation, we can demonstrate that the ratio of the stresses due to the extensional viscosity to the shear viscosity is given by $\frac{\mu'_E}{\mu'_1}\left(\frac{h'}{l'}\right)^2$, where h' is the gap between the surfaces (≈100 µm, Figure 10). The value of this ratio is about 0.01 (<<1). We can conclude that extensional effects of saliva should have a slight effect on the coating of mucosa.

The shear of saliva induces normal stress effects (Stokes et al., 2007) that could participate to support the load L' applied by the constrictor muscles. Normal stress N_1' is about 10-100 Pa for shear stresses comprise between 10 and 2000 s^{-1} (Stokes et al., 2007). In the contact between the roots of the tongue and the posterior pharyngeal wall, these effects could generate a load L_{N1}' given by N_1'.l', approximately. An order of magnitude of L_{N1}' is 1 N/m. This value represents only 10% of the load L' applied by the constrictor muscles. We can so conclude that the normal stress effects of saliva must have a moderate effect on the coating phenomena during swallowing.

Thus, at the light of the simulations obtained with the present model, we can conclude that the shear thinning behavior and the viscoelasticity of saliva should affect mucosa coating phenomena and would be interesting to study in detail. However, these phenomena could affect the results only

quantitatively. In fact, qualitatively, the existence of the two sets of conditions demonstrated in this study is due to obstructions effects by saliva. Moreover, the behavior law of saliva has to be determined on a large scale of shear rates that is difficult to obtain experimentally and the effect of viscoelasticty on lubrication-flows characteristics is a "largely-unresolved problem" (Zhang and Li, 2005).

5.2. Rheology of food bolus

A second interesting question is the role of food bolus rheology on coating phenomena. Food bolus can present all kind of rheological properties from liquid to semi-solid food products or chewing solid food. In the present model, we choose to only explore the viscous effects in order to not over-sophisticate the model and to be representative of the experimental conditions of Doyennette et al. (2011) and compare thus the results of these two different approaches.

However, as saliva, it is clear that more complex rheological properties can impact on coating phenomena. For example, biopolymers and hydrocolloids used as thickeners present shear thinning behaviors. Food bolus can also present a yield stress. The yield stress effects and the shear thinning behavior can have a great impact on the coating phenomena because the shear rates generated in the contact vary from 0 to 10^4 s^{-1}. It could be interesting to develop a specific experimental device as in our previous study (de Loubens et al., 2010) with deformable rolls to study the influence of complex rheological properties on coating (as inhomogeneous food bolus for example). To study pharyngeal mucosa coating, modeling stays an interesting approach because it allows us to evaluate physical quantities that are very difficult to measure *in vivo*.

6. Conclusion

To conclude, the elastohydrodynamic model of swallowing provides physical explanations as to the role of saliva on the food bolus coating and flavour release. After being successfully compared with *in vivo* experiments, this type of approach is promising for designing food products with specific aroma

release kinetics or for adapting food product properties to people who suffer from swallowing disorders. However, the food bolus presents complex behaviours and the development of *in vitro* systems to model swallowing may be of great interest for studying the role of the rheological properties of the food bolus on the pharyngeal mucosa coating and flavour release.

Acknowledgments

The authors gratefully acknowledge the French National Research Agency (ANR) project SensInMouth for financial support.

Disclosures

No conflicts of interest, financial or otherwise, are declared by the authors.

References

Boland, A., Delahunty, C., et van Ruth, S. (2006). Influence of the texture of gelatin gels and pectin gels on strawberry flavour release and perception. Food Chemistry, 96(3) :452–460.

Buettner, A., Beer, A., Hannig, C., Settles, M., 2001. Observation of the swallowing process by application of videofluoroscopy and real-time magnetic resonance imaging-consequences for retronasal aroma stimulation. Chemical Senses 26 (9), 1211–1219.

Carvalho, M., Scriven, L., 1995. Deformable roll coating: Modeling of steady flow in gaps and nips. In: P.H. Gaskell, M. S. . J. S. (Ed.), The Mechanics of Thin Film Coating: Proc. First European Symp. World Scientific, pp. 221–230.

Chang, M., Rosendall, B., Finlayson, B., 1998. Mathematical modeling of normal pharyngeal bolus transport: A preliminary study. Journal of Rehabilitation Research and Development 35 (3), 327–334.

Chong, Y., Gaskell, P., Kapur, N., 2007. Coating with deformable rolls: An experimental investigation of the ribbing instability. Chemical Engineering Science 62 (15), 4138 – 4145.

402 Cohu, O., Magnin, A., 1997. Forward roll coating of Newtonian fluids with deformable rolls: An
403 experimental investigation. Chemical Engineering Science 52 (8), 1339–1347.

404 Cook, D., Hollowood, T., Linforth, R., Taylor, A., 2003. Oral shear stress predicts flavour perception in
405 viscous solutions. Chemical Senses 28 (1), 11–23.

406 Coyle, D.J., 1988. Forward roll coating with deformable rolls - a simple one-dimensional
407 elastohydrodynamic model. Chemical Engineering Science 43 (10), 2673–2684.

408 Dantas, R., Kern, M., Massey, B., Dodds, W., Kahrilas, P., Brasseur, J., Cook, I., Lang, I., 1990. Effect of
409 swallowed bolus variables on oral and pharyngeal phases of swallowing. American Journal of
410 Physiology 258 (5, Part 1), G675–G681.

411 de Loubens, C., Magnin, A., Verin, E., Doyennette, M., Tréléa, I.C., Souchon, I., 2010. A lubrication
412 analysis of the pharyngeal peristalsis: application to flavour release. Journal of Theoretical Biology
413 267 (3), 300–311.

414 Diridollou, S., Patat, F., Gens, F., Vaillant, L., Black, D., Lagarde, J., Gall, Y., Berson, M., 2000. In vivo
415 model of the mechanical properties of the human skin under suction. Skin Research and Technology
416 6 (4), 214–221.

417 Doyennette, M., de Loubens, C., Déléris, I., Souchon, I., Tréléa, I.C., 2011. Mechanisms explaining the
418 role of viscosity and post-deglutitive pharyngeal residue on in vivo aroma release: a combined
419 experimental and modeling study. Food Chemistry. doi:10.1016/j.foodchem.2011.03.039

420 Gostling, M., Savage, M., Young, A., Gaskell, P., 2003. A model for deformable roll coating with
421 negative gaps and incompressible compliant layers. Journal of Fluid Mechanics 489, 155–184.

422 Haward, S.J., Odell, J.A., Berry, M., Hall, T., 2010. Extensional rheology of human saliva. Rheological
423 Acta, doi: 10.1007/s00397-010-0494-1.

424 Hollowood, T., Linforth, R., Taylor, A., 2002. The effect of viscosity on the perception of flavour.
425 Chemical Senses 27 (7), 583–591.

426 Johnson, K. L., 1970. Regimes of elastohydrodynamic lubrication. Journal of Mechanical Engineering
427 Science 12, 9.

428 Kim, S., McCulloch, T., Rim, K., 1998. Evaluation of the viscoelastic properties of pharyngeal tissue.
429 Tissue Engineering 4 (4), 389–401.

430 Levine, M., 1989. Radiology of the esophagus. WB Saunders, Philadelphia.

431 Meng, Y., Rao, M., Datta, A., 2005. Computer simulation of the pharyngeal bolus transport of
432 Newtonian and non-Newtonian fluids. Food and Bioproducts Processing 83 (C4), 297–305.

433 Pal, A., Williams, R., Cook, I., Brasseur, J., 2003. Intrabolus pressure gradient identifies pathological
434 constriction in the upper esophageal sphincter during flow. American Journal of Physiology
435 Gastrointestinal and Liver Physiology 285 (5), G1037–G1048.

436 Saint-Eve, A., Martin, N., Guillemin, H., Semon, E., Guichard, E., Souchon, I., 2006. Flavored yogurt
437 complex viscosity influences real-time aroma release in the mouth and sensory properties. Journal of
438 Agricultural and Food Chemistry 54 (20), 7794–7803.

439 Schipper, R. G., Silletti, E., Vinyerhoeds, M. H., 2007. Saliva as research material: Biochemical,
440 physicochemlical and practical aspects. Archives of Oral Biology 52 (12), 1114–1135.

441 Skotheim, J., Mahadevan, L., 2005. Soft lubrication: The elastohydrodynamics of nonconforming and
442 conforming contacts. Physics of Fluids 17 (9).

443 Stokes, J.R., Davies, G.A., 2007. Viscoelasticticy of human whole saliva collected after acid and
444 mechanical stimulation. Biorheology 44, 141-160.

445 Taniguchi, H., Tsukada, T., Ootaki, S., Yamada, Y., Inoue, M., 2008. Correspondence between food
446 consistency and suprahyoid muscle activity, tongue pressure, and bolus transit times during the
447 oropharyngeal phase of swallowing. Journal of Applied Physiology 105 (3), 791–799.

448 Tréléa, I., Atlan, S., Déléris, I., Saint-Eve, A., Marin, M., Souchon, I., 2008. Mechanistic mathematical
449 model for in vivo aroma release during eating of semiliquid foods Chemical Senses 33, 181-192.

450 Tsukada, T., Taniguchi, H., Ootaki, S., Yamada, Y., Inoue, M., 2009. Effects of food texture and head
451 posture on oropharyngeal swallowing. Journal of Applied Physiology 106 (6), 1848–1857.

452 Weel, K., Boelrijk, A., Burger, J., M., V., Gruppen, H., Voragen, A., Smit, G., 2004. New device to
453 simulate swallowing and in vivo aroma release in the throat from liquid and semiliquid food systems.
454 Journal of Agricultural and Food Chemistry 52 (21), 6564–6571.

455 Woda, A., Mishellany-Dutour, A., Batier, L., Francois, O., Meunier, J.-P., Reynaud, B., Alric, M.,
456 Peyron, M.-A., 2010. Development and validation of a mastication simulator. Journal of Biomechanics
457 43 (9), 1667 – 1673.

458 Yven, C., Guessasma, S., Chaunier, L., Valle, G. D., Salles, C., 2010. The role of mechanical properties
459 of brittle airy foods on the masticatory performance. Journal of Food Engineering 101 (1), 85 – 91.

460 Zhang, R., LI, X.K, 2004. Non-Newtonian effects on lubricant thin film flows. Journal of Engineering
461 Mathematics, 51: 1–13.

462

463

464 Table 1: Physiological variables and approximate corresponding values.

Description	Symbol	Typical values	References
Saliva thickness	e_1'	no data	
Saliva viscosity	μ_1'	1 1-10 mPa.s	Schipper et al., 2007; Stokes et al., 2007
Bolus viscosity	μ_2'	> 1 mPa.s	
Wave velocity	U'	0.1-0.5 m/s	Dantas et al., 1990; Meng et al., 2005; Chang et al., 1998
Radius	R'	40 mm	estimated from Chang et al., 1998
Elasticity modulus of the mucosa	E'	20-200 kPa	Diridollou et al., 2000; Kim et al., 1998
Mucosa thickness	e_m'	1-4 mm	Diridollou et al., 2000
Load	L'	10-60 N/m	de Loubens et al., 2010
Elasticity parameter	E_S	$\sim 8.10^{-9}$	calculated with (1)
Load parameter	F	$\sim 3.10^{-5}$	calculated with (2)

465

466

467

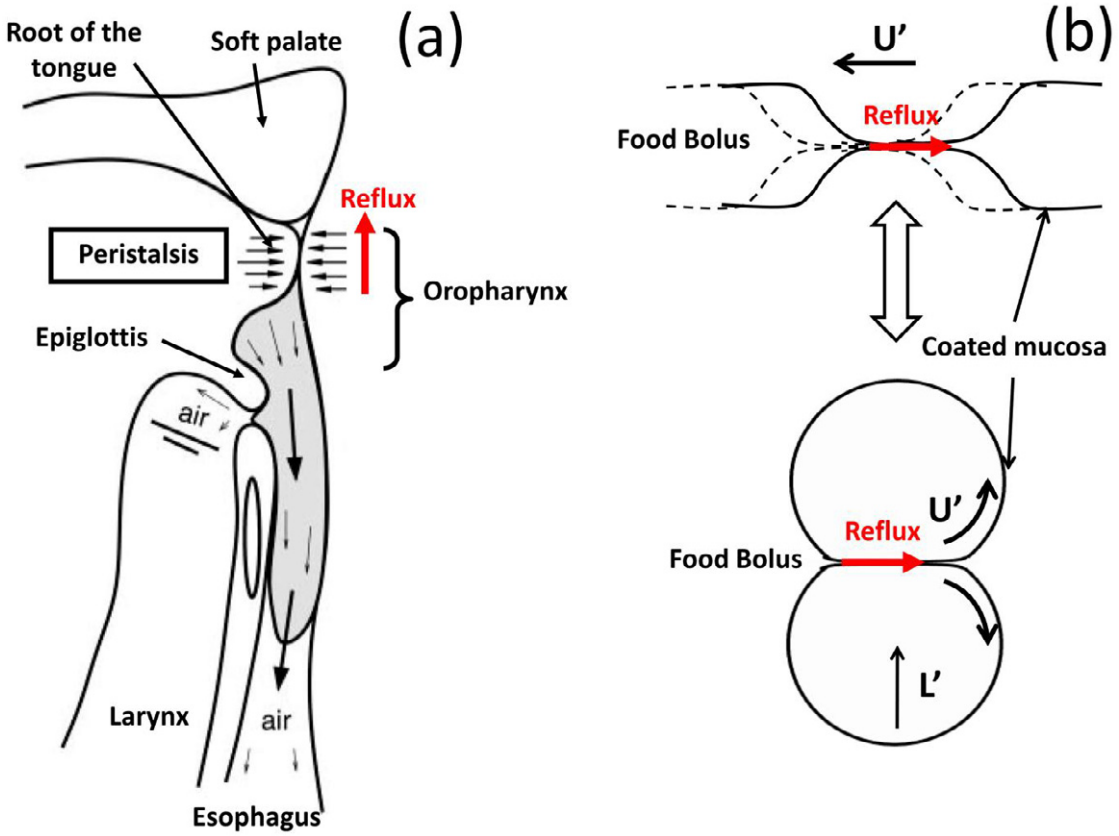

Figure 1: (a) Pharyngeal peristalsis (adapted from Pal et al., 2003). (b) Diagram of the peristaltic wave and associated study system. Near the most occluded point, the pharyngeal walls are in rotation compared to each other. U' is the wave velocity (m/s) and L' the load applied by the pharyngeal constrictors muscles (N/m), adapted from de Loubens et al. (2010).

475

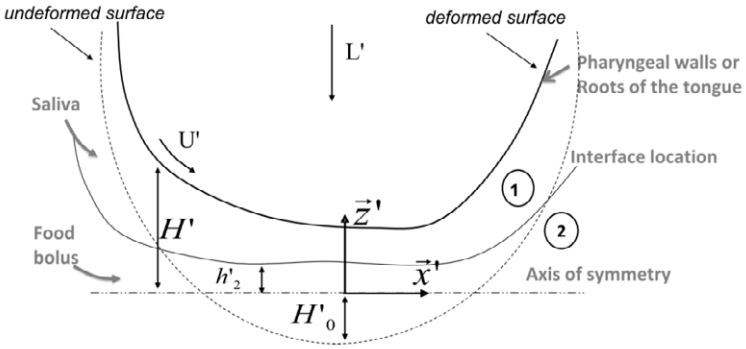

476

477 Figure 2: Diagram of definition and notations. U' is the wave velocity (m/s), L' the load applied by the

478 pharyngeal constrictors muscles (N/m), H'(x') the mucosa location (m), h_2' (x') the interface location

479 between the food bolus and the saliva and H_0' the negative-gap width.

480

481

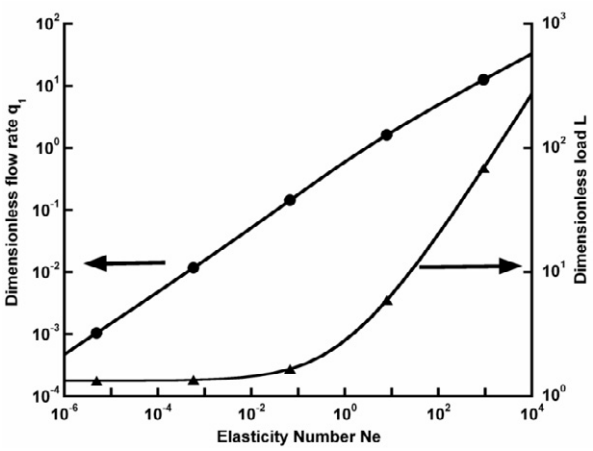

482

483 Figure 3: Dimensionless flow rate q_1 (-●-) and load L (-▲-) as a function of the elasticity number N_e in

484 the mono-layer case (q_2=0).

485

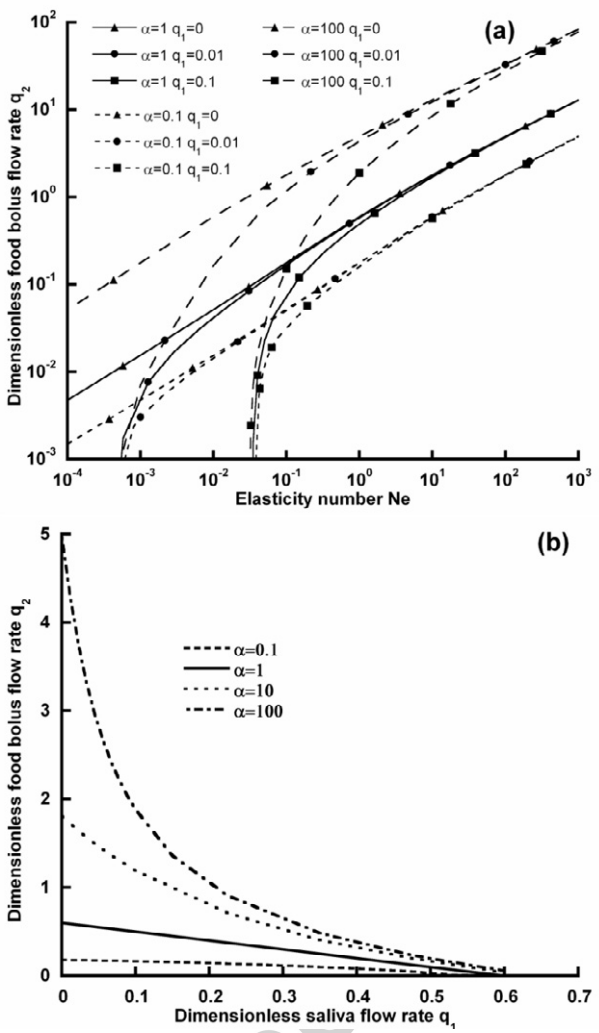

Figure 4: Dimensionless food bolus flow rate q_2 as a function of the elasticity number N_e for different viscosity ratios α and dimensionless saliva flow rates q_1 (a) and as a function of dimensionless saliva flow rate q_1 for different viscosity ratios α for N_e=1 (b).

492

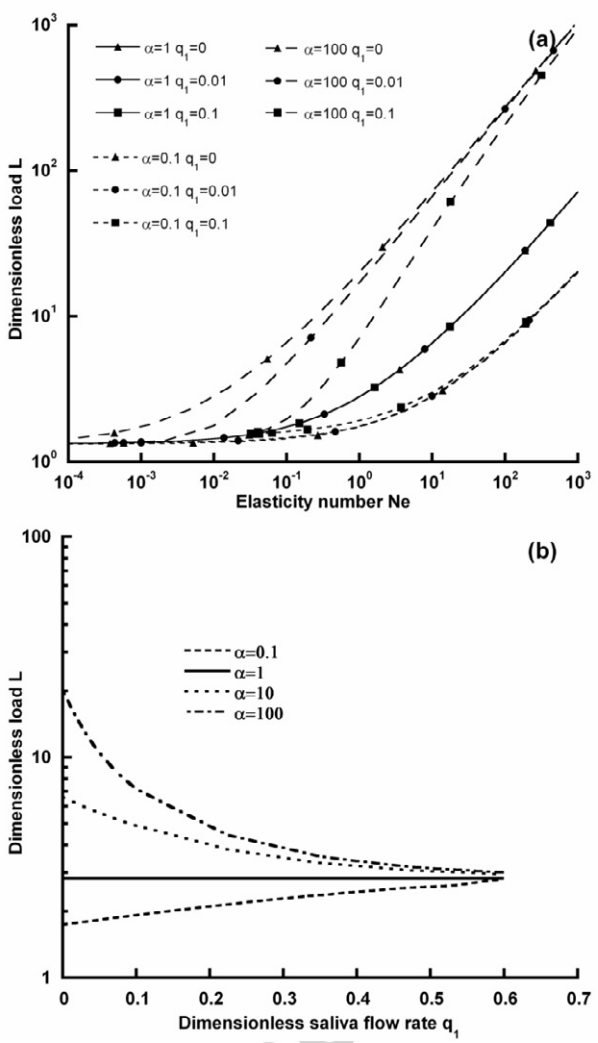

493

494 Figure 5: Dimensionless load L as a function of the elasticity number N_e for different viscosity ratio α

495 and dimensionless saliva flow rates q_1 (a) and as a function of the dimensionless saliva flow rate for

496 different viscosity ratios α at imposed gap and velocity for N_e=1 (b).

497

498

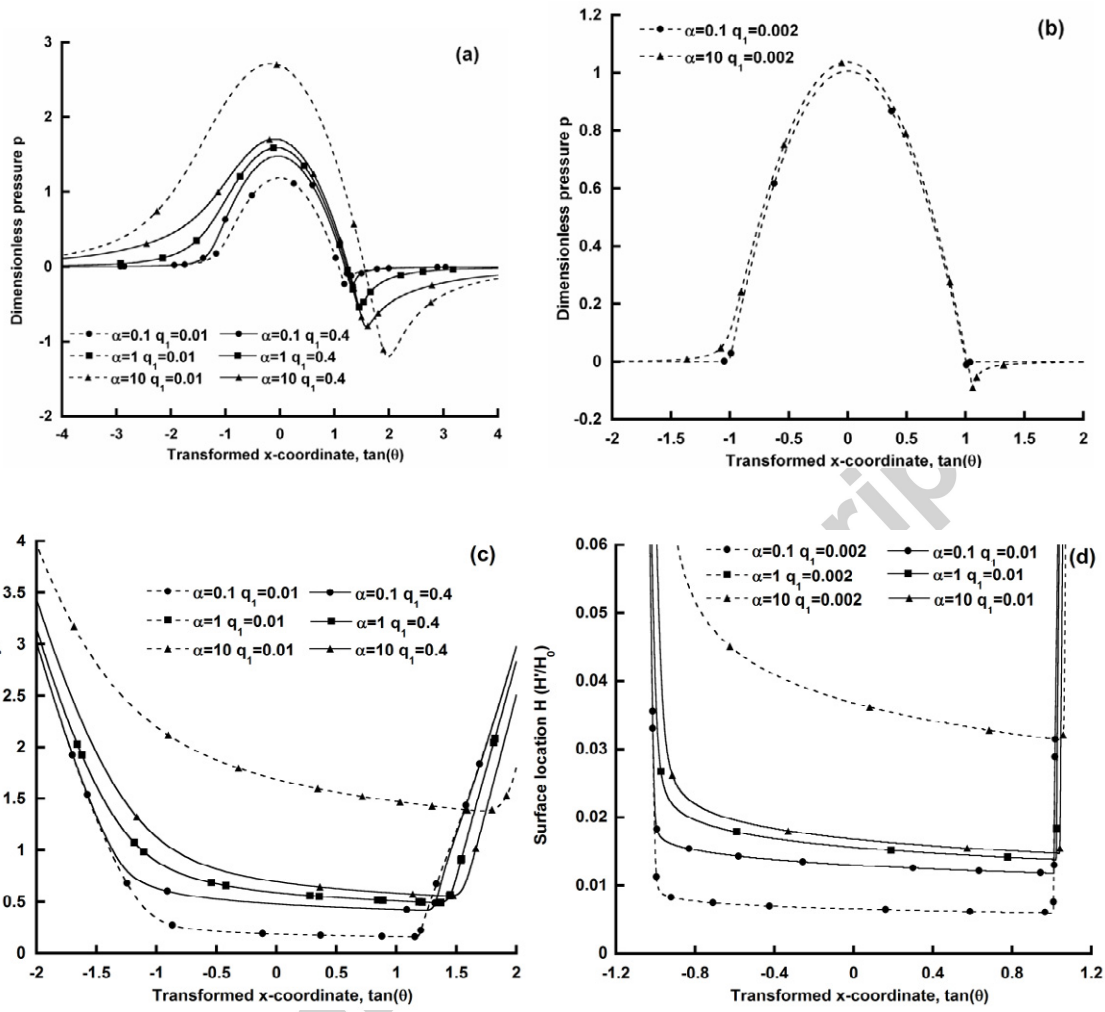

499

500

501 Figure 6: Dimensionless pressure profiles p (a and b) and gap profiles H (c and d) for different

502 viscosity ratio α and different dimensionless saliva flow rates q_1 at N_e=1 (a and c) and N_e=10^{-3} (b and

503 d).

504

505

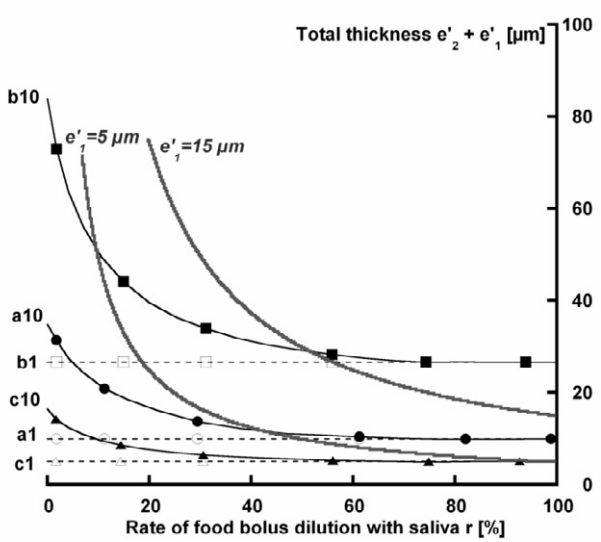

506

Cas n°	U' [m/s]	E' [kPa]	μ_2' [mPa.s]	α	E_s	F
a1 (○)	0.1	20	5	1	$4\ 10^{-9}$	$8\ 10^{-5}$
a10 (●)	0.1	20	50	10	$4\ 10^{-9}$	$8\ 10^{-5}$
b1 (□)	0.5	20	5	1	$2\ 10^{-8}$	$8\ 10^{-5}$
b10 (■)	0.5	20	50	10	$2\ 10^{-8}$	$8\ 10^{-5}$
c1 (Δ)	0.1	200	5	1	$4\ 10^{-10}$	$8\ 10^{-6}$
c10 (▲)	0.1	200	50	10	$4\ 10^{-10}$	$8\ 10^{-6}$

507

508 Figure 7: Total thickness of food bolus and saliva e'=e_1'+e_2' coating the pharyngeal mucosa as a

509 function of the dilution rate of the food bolus with saliva $r = 100\,\frac{e_2'}{e_1'+e_1'}$ and iso-values of saliva

510 thickness e_1' (grey lines) (e_m'=4 mm, R'=4 mm,μ_1'=5 mPa.s, L'=10 N/m).

511

512

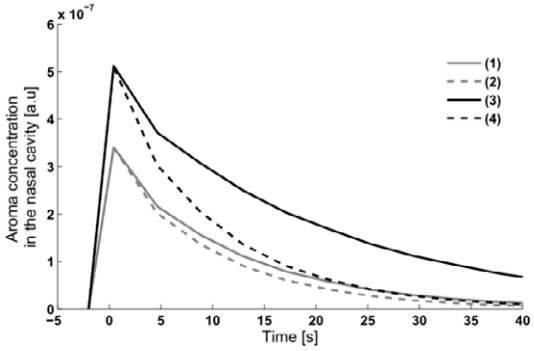

513

Cas n°	α	r (%)	e'$_2$+e'$_1$
1	10	40	12
2	1	40	10
3	10	10	20
4	1	10	10

514

515 Figure 8: Aroma release kinetics predicted by the mechanistic model developed by Doyennette et al.

516 (2011) for different rates of dilution of the food bolus with saliva ($r = 100\,\frac{e_2'}{e_1'+e_1'}$) and total

517 thicknesses (e$_1$'+e$_2$') predicted with the present elastohydrodynamic model. The time 0 s corresponds

518 to the swallowing events. (U'=0.5 m/s, E'=20 kP a, e$_m$'=4 mm, R'=4 mm,μ_1'=5 mPa.s, L'=10 N/m)

519

520

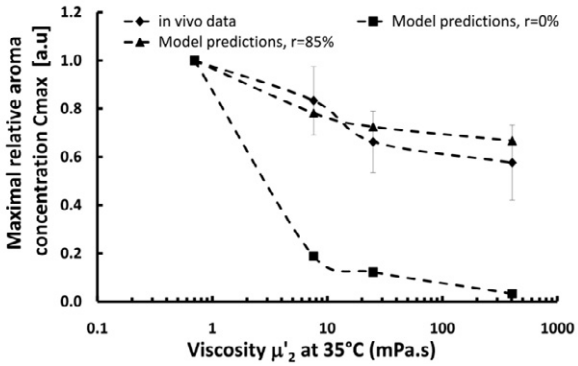

521

522 Figure 9: Maximal relative concentration of aroma release kinetics C_{max} as a function of the viscosity
523 of glucose solutions μ_2': *in vivo* data (♦), model predictions without dilution with saliva (r=0%,■),
524 model predictions with a rate of dilution of product with saliva r of 85% (▲). Error bars represent the
525 standard deviation on the in vivo data. Data from Doyennette et al. (2011).

526

527

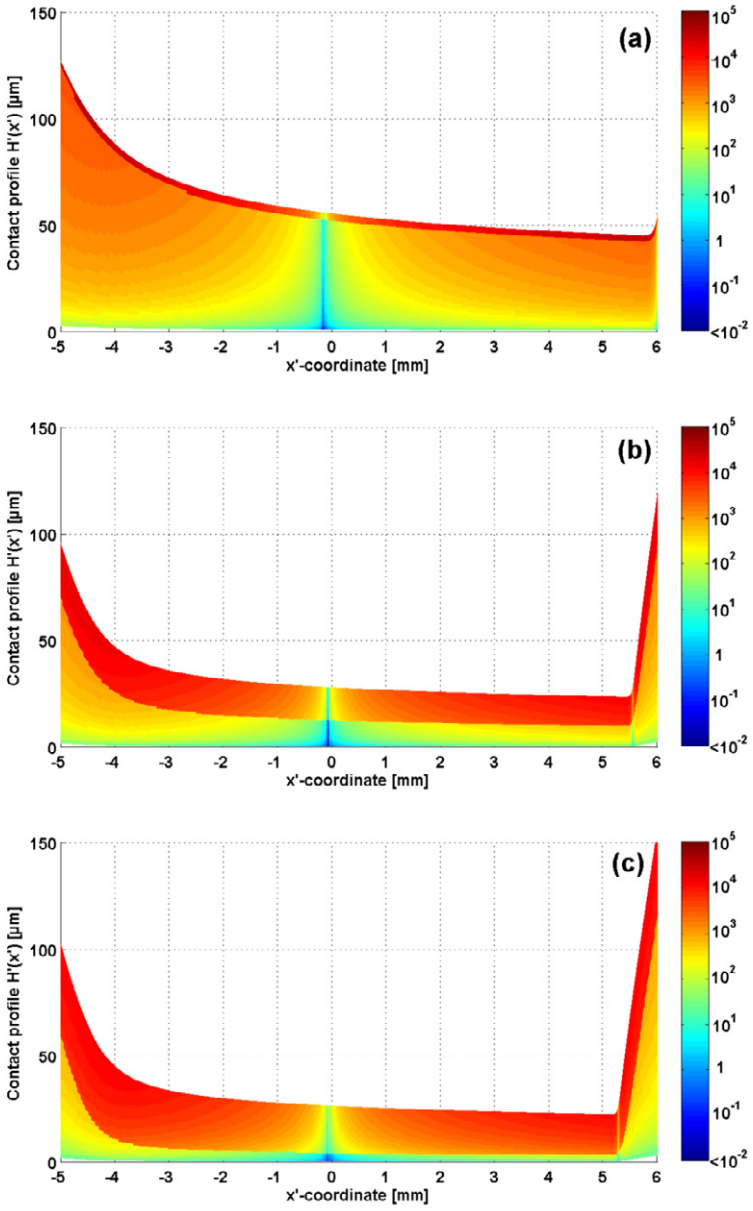

528

529 Figure 10: Example of shear rate distribution (isovalues of shear rate in 1/s) in the contact for
530 different level of saliva lubrication: e_1=2.6 µm and e_2=61 µm (a), e_1=13 µm and e_2=17 µm (b),
531 e_1=22 µm and e_2=4.2 µm (c). The z'-coordinate 0 correspond to the axis of symmetry (U'=0.5 m/s,
532 E'=20 kP a, e_m'=4 mm, R'=4 mm,μ_1'=5 mPa.s, μ_2'=10 mPa.s, L'=10 N/m).

Highlights

We modeled pharyngeal peristalsis.

We analysed the great role of saliva and mucosa deformabilty on mucosa coating by Newtonian food bolus.

We concluded that the food bolus coating the mucosa is very diluted by saliva during the swallowing process.

Thus the impact of product viscosity on flavor release is weak.